

Development and Validation of a Finite Element Model of the Human Middle Ear Based on Medical Imaging

Souad Elghanaoui^{1}, Adil Faiz², Safa Assif¹, and Abdelowahed Hajjaji¹*

¹Laboratory of Engineering Sciences for Energy, Research Axis: Computational Mechanics and Acoustics, National School of Applied Sciences, Chouaib Doukkali University, El Jadida, Morocco

²Laboratory of Energetics and Theoretical and Applied Mechanics, Lorraine University, Nancy, France

Abstract. Finite-element modeling (FEM) is a powerful tool for studying the mechanical behavior of the human ear. This study presents a three-dimensional FEM of the middle and inner ear, developed from high-resolution computed tomography (CT) data. The model includes the external auditory canal, tympanic membrane, and ossicular chain, with the inner ear represented as a viscous damping element. Frequency-domain simulations were performed to analyze tympanic membrane and stapes vibrations. Results show strong agreement with experimental data, demonstrating that the proposed FEM accurately reproduces middle ear dynamics across a wide frequency range. The methodology provides a reliable framework for investigating auditory mechanics and designing biomedical devices.

Keywords: Finite Element Modeling, Middle Ear Mechanics, Radiological Imaging, Tympanic Membrane Vibration, Ossicular Chain Dynamics

1 Introduction

The human ear is a highly intricate organ, and its response to sound is far from simple. Understanding this behavior is essential not only for explaining normal hearing but also for clarifying how various disorders may alter it. Over the past few decades, the finite element method (FEM) has been increasingly applied to create digital models of the ear. Some studies relied on simplified two-dimensional representations of the outer ear, often reducing the ear canal to a symmetric tube [1], [2], [3]. Others advanced toward three-dimensional models of the middle ear, but their accuracy was limited by the scarcity of precise anatomical data [4], [5].

* Corresponding author: elghanaoui.s@ucd.ac.ma

Several research efforts have contributed to the development of FEM models of the middle ear. Koike et al. [4] reproduced the geometry of the tympanic membrane and ossicles from previously published measurements. While useful, this approach provided only a partial and simplified description of the middle ear anatomy. Later, Gan et al. [6] and Sun et al. [5] employed histological sectioning to reconstruct detailed three-dimensional geometries of the middle ear. Although these techniques offered a high level of anatomical detail, they were inherently destructive and risked introducing tissue deformation or spatial inconsistencies between structures.

In this work, we present an alternative approach based on high-resolution computed tomography imaging. This non-destructive method enables the reconstruction of a complete and anatomically coherent three-dimensional model of the middle ear, including the ossicular chain, tympanic membrane, and supporting structures. Integrating this geometry into a finite element framework provides a more reliable and realistic tool for mechanical simulation compared to previous reconstruction techniques.

The objective of this study is to develop and validate a finite element model of the human middle ear derived from high-resolution CT data, with the goal of achieving a more anatomically accurate and mechanically robust representation of sound transmission

2 METHODS

We started by reconstructing the 3D geometry of the human ear using radiological images. Once the geometry was established, the various tissue regions were imported into COMSOL Multiphysics (COMSOL, Sweden) for finite element analysis. Material characteristics were attributed to each component, boundary conditions were applied, and a mesh was created to discretize the model before proceeding with the numerical solution.

2.1 Geometric Model

We started from high-resolution CT scans of the head of a healthy adult male, acquired using a Rochet scanner to build a three-dimensional representation of the auditory system. The images were processed in 3D Slicer to reduce noise, adjust intensity and contrast, and remove artifacts before moving on to the segmentation phase.

The reconstruction process started with the ossicular chain. The malleus, incus, and stapes were carefully identified on the CT images by examining each slice. Because of their complex shapes and close proximity to other bone structures, segmentation was done manually to ensure accuracy. Each ossicle's outline was traced precisely across the different image planes to capture their detailed anatomy and connections (Fig 1).

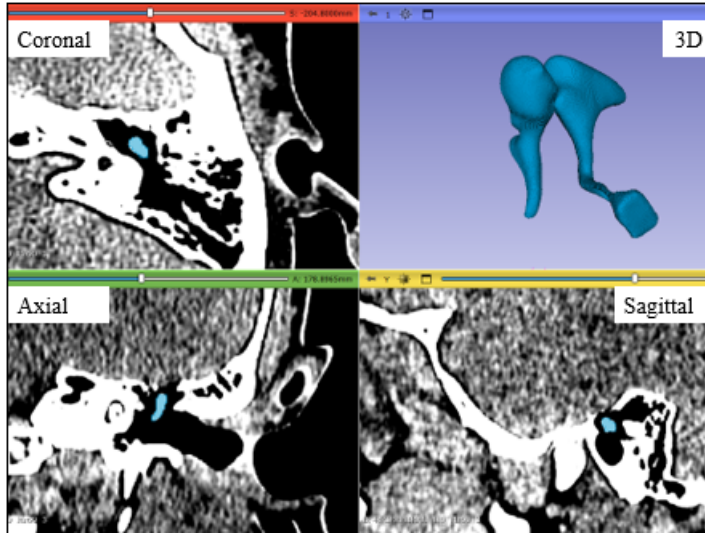


Fig. 1. Radiological image of the human middle ear obtained by computed tomography.

The geometric reconstruction of the auditory canal was established through automatic segmentation the region corresponding to the external auditory canal was isolated by defining an appropriate range of Hounsfield units to differentiate air-filled spaces from surrounding bone tissue. Threshold-based segmentation was applied, followed by manual corrections in axial, sagittal, and coronal views to refine the canal's boundaries and remove unwanted connections with adjacent cavities. The resulting mask was then smoothed to reduce stair-step artifacts from the slice thickness. Finally, a three-dimensional surface model of the canal cavity was generated, providing an accurate geometric representation of its curvature and cross-sectional variations (Fig 2).

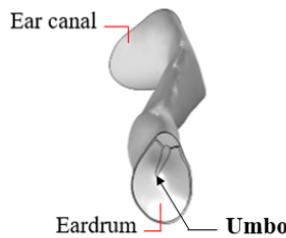


Fig. 2. Auditory canal model. The model includes the external auditory canal, the tympanic membrane, and the umbo, located at the central point of maximum concavity of the tympanic membrane.

The eardrum, which is not clearly visible on the CT scans due to its thinness, was approximated using adjacent surfaces of the auditory canal. It was modeled as three distinct layers—the pars flaccida, pars tensa, and tympanic ring—each assigned a uniform thickness of 74 μm . This value is consistent with measurements reported in the literature [7], [8]. Although the assumption of uniform thickness is a simplification, it allows a manageable yet realistic representation of the membrane in the FEM model while maintaining the correct mechanical behavior observed in experimental studies. The tympanic ring was represented as a curved structure encircling only the pars tensa,

splitting into two branches at the tympanic spines: an anterior branch forming the anterior tympanomalleolar ligament and a lateral branch forming the posterior tympanomalleolar ligament, both connecting to the malleus (Fig. 3). This layered approach captures the main mechanical interactions within the eardrum while remaining computationally efficient.

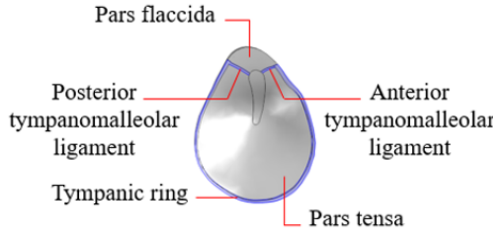


Fig. 3. Eardrum model. The model includes the pars tensa, pars flaccida, and the tympanic ring surrounding the pars tensa, as well as the anterior and posterior tympanomalleolar ligaments.

Five middle ear ligaments—anterior, superior, and lateral malleolar, plus superior and posterior incudal—were included, along with the tensor tympani and stapedial tendons (Fig. 4), using reported anatomical dimensions [9].

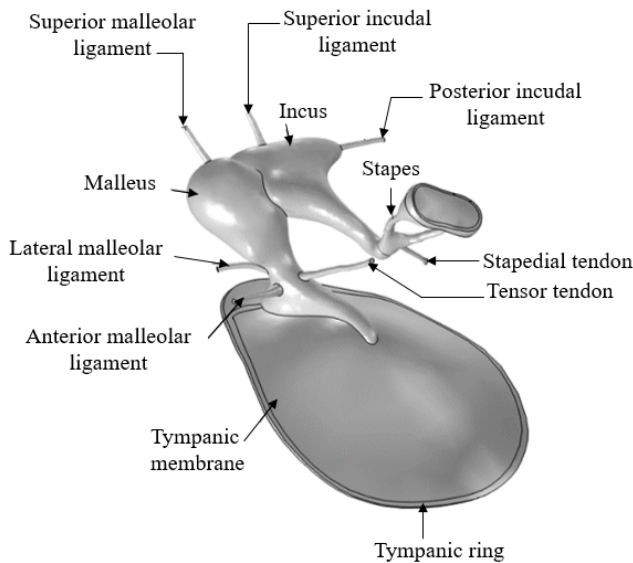


Fig. 4. Middle ear model. The model includes the tympanic membrane, ossicles, and supporting ligaments.

The stapedial annular ligament was modeled as an elliptical band encircling the stapes footplate [10] (Fig. 5). The malleus and incus were treated as a rigid unit, while the incudo-stapedial joint was represented as an elliptical interface between the incus and stapes, reflecting its role in sound transmission.

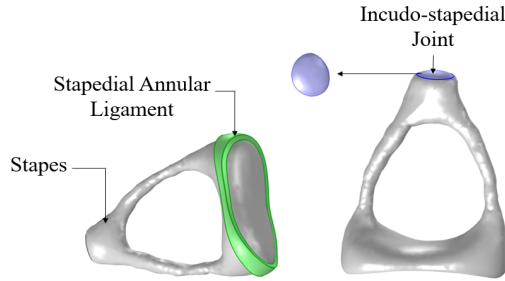


Fig. 5. Stapedial annular ligament and incudo-stapedial joint.

2.2 Finite Element Modeling

After constructing the 3D geometry of our model, we proceeded with finite element modeling. Material properties were assigned to the various components of the model, assuming that all materials used are linear elastic. We used the same density and Young's modulus values as Koike et al. [4], which helps keep our model consistent with existing studies and allows for better comparison. Each part of the ear was assigned these properties individually. We also used a Poisson's ratio of 0.3 for all tissues, a typical value used in the literature [11].

When it came to boundary conditions, we made sure to reflect the actual physical constraints inside the ear. The domains of the auditory canal and middle ear that are in contact with air were treated as free surfaces, meaning these areas could move freely without any external forces acting on them [12]. On the other hand, the ligaments, tendons, and the edges of the pars flaccida, tympanic ring, and stapedial annular ligament were fixed in place to represent their solid attachment to the temporal bone [4].

To account for energy dissipation in the middle ear, Rayleigh damping was applied to all structures, with parameters set at $\alpha = 0 \text{ s}^{-1}$ and $\beta = 0.75 \times 10^{-4} \text{ s}$, based on prior studies [6], [8]. While simplified, these parameters provide a realistic approximation of tissue damping by combining viscous and structural effects. Additionally, the cochlear fluid was modeled as a viscous damper applied to the stapes footplate (Fig. 6), simulating the resistance offered by the cochlea during sound transmission. Although this does not fully capture the complex fluid-structure interactions within the cochlea, it reproduces the main mechanical effect of cochlear loading on stapes motion, which is sufficient for assessing the overall middle ear vibration patterns.

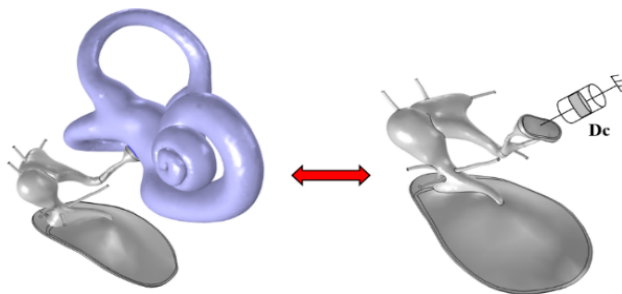


Fig. 6. Inner ear model. With $D_c = 0.2 \text{ N.s/m}$, the viscous damping coefficient applied to the stapes footplate [6] to model the mechanical effect of the cochlear fluid.

3 Results and Discussion

The finite element model was validated by comparing the umbo and stapes footplate displacements with numerical results previously published by Koike et al. [4] and experimental measurements reported by Gyo et al. [13]. To complement this qualitative assessment, a quantitative comparison was conducted between our CT-based FEM model, Koike et al.'s model [4], and the experimental data from Gyo et al. [13]. This analysis assesses the accuracy of each model in reproducing experimental measurements across the frequency range of 200–2000 Hz, which encompasses the most relevant frequencies for human hearing and middle ear resonance.

3.1 Eardrum Displacement

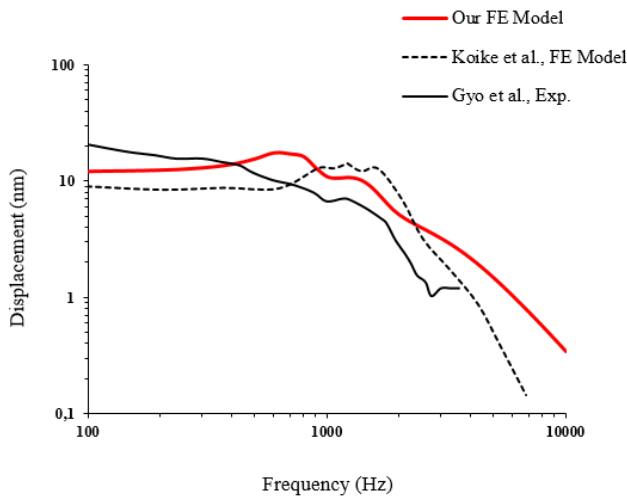


Fig. 7. Frequency response of umbo displacement. The red curve represents the results from the present FEM model, the black dashed curve shows the numerical simulation reported by Koike et al. [4], and the black solid curve corresponds to experimental measurements from Gyo et al. [13].

Figure 7 summarizes the frequency-dependent displacement of the umbo obtained from our simulations. Key features are:

- From low frequency up to about 700 Hz the umbo displacement is essentially flat, with an average amplitude near 12 nm.
- Between ~700 Hz and around 2000 Hz the amplitude increases, reaching a pronounced peak close to 2000 Hz.
- Above the peak the displacement steadily declines as frequency increases.

This behaviour is consistent with a resonance of the coupled eardrum–ossicular chain: at low frequencies the system is stiffness-controlled and transmits sound with relatively uniform gain, while near the natural resonance the effective transfer is amplified because the inertia and compliance of the membrane and ossicles interact constructively. The

subsequent drop at higher frequencies reflects the transition toward inertial domination and increased damping of higher-order structural modes [14].

The close alignment between our model's displacement curve and that of Koike et al. [4], both showing a peak between 700 and 2000 Hz, supports the validity of our approach.

This consistency indicates that our model captures the principal mechanical coupling and modal behaviour of the middle ear.

Minor differences between the curves can be primarily attributed to anatomical variations considered in each study, particularly the geometry of the middle ear structures, which influence the dynamic response. Additionally, certain model simplifications, such as assumptions regarding the tympanic membrane thickness or the choice of boundary conditions, may also contribute to small discrepancies in the results.

3.2 Stapes Displacement

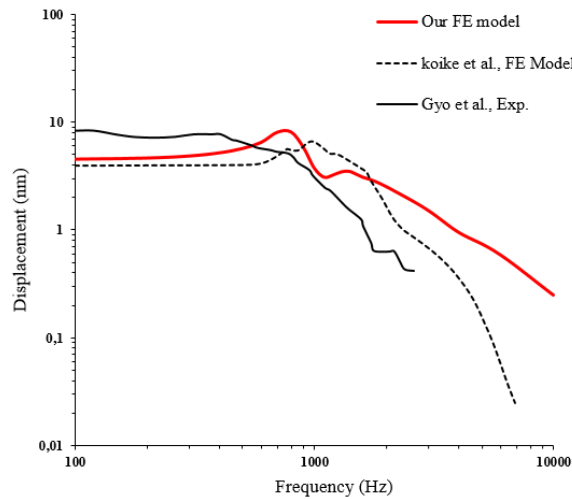


Fig. 8. Frequency response of stapes displacement. The red curve represents the results from the present FEM model, the black dashed curve shows the numerical simulation reported by Koike et al. [4], and the black solid curve corresponds to experimental measurements from Gyo et al. [13].

Figure 8 present the numerically calculated displacements of the stapes. Our findings reveal that the stapes displacement remains nearly constant at about 4.5 nm until 700 Hz. Above this frequency, the displacement increases, reaching a peak around 1000 Hz, before gradually declining as the frequency continues to rise. The displacement curve from our model closely matches that of Koike et al. in the low to mid-frequency range, featuring a peak between 700 and 2000 Hz.

However, above 2000 Hz, more noticeable differences appear between our results and both experimental and numerical data. This discrepancy is mainly due to our model not including the load from the intracochlear fluid mass on the stapes footplate, because of limited anatomical data. As Wilson [14] points out, the middle ear's behavior at high frequencies is largely governed by the system's mass.

3.3 Comparaison quantitative

To complement the qualitative assessment, a quantitative error analysis was performed by comparing the displacements obtained from our model, Koike et al.'s model [4], and the experimental measurements of Gyo et al. [13]. Tables 1 and 2 present the frequency-dependent displacements of the umbo and stapes, along with the relative deviation (in %) of each model with respect to Gyo et al.'s experimental data. These pointwise deviations allow assessing how closely each model follows the experimental trends across the frequency range of 200–2000 Hz, which was chosen because it corresponds to the essential range of human hearing, including the primary resonance region of the tympano-ossicular chain and the critical frequencies for speech perception and understanding.

The pointwise deviation is calculated as:

$$\text{Deviation (\%)} = \frac{X_{\text{model}} - X_{\text{exp}}}{X_{\text{exp}}} \times 100 \tag{1}$$

where X_{model} is the displacement computed by the FEM model (either our model or Koike et al.'s) and X_{exp} is the experimentally measured displacement reported by Gyo et al.

Table 1. Umbo displacement (nm) and relative deviation compared to experimental measurements

Frequency (Hz)	Gyo et al.	Our model	Koike et al. Model	Deviation (%) (Our model vs Exp)	Deviation (%) (Koike vs Exp)
200	16.38	12.19	8.26	-25.6 %	-49.6 %
400	13.74	14.39	8.61	+4.8 %	-37.3 %
600	9.88	17.30	8.59	+75.0 %	-13.1 %
800	8.57	15.98	10.66	+86.4 %	+24.4 %
1000	6.57	10.64	12.62	+62.0 %	+92.1 %
1200	6.77	10.46	12.81	+54.5 %	+89.2 %
1400	5.70	9.52	12.02	+67.0 %	+111.0 %
1600	4.80	7.42	12.39	+54.5 %	+158.2 %
1800	3.62	5.69	9.21	+57.0 %	+154.6 %
2000	2.65	5.02	6.74	+89.3 %	+154.5 %

Table 2. Stapes footplate displacement (nm) and relative deviation compared to experimental measurements

Frequency (Hz)	Gyo et al.	Our model	Koike et al. model	Deviation (%) (Our model vs Exp)	Deviation (%) (Koike vs Exp)
200	7.28	4.77	3.93	-34.4 %	-45.9 %
400	7.93	5.39	4.00	-32.0 %	-49.6 %
600	5.94	6.71	4.25	+13.1 %	-28.4 %
800	5.01	8.20	5.77	+63.6 %	+15.1 %
1000	3.19	3.87	6.68	+21.2 %	+109.3 %
1200	2.29	3.32	5.15	+44.7 %	+124.6 %
1400	1.77	3.57	4.41	+102.3 %	+149.6 %
1600	1.32	3.28	3.71	+149.3 %	+182.2 %
1800	0.74	3.01	2.53	+308.1 %	+242.4 %

2000	0.65	2.67	1.69	+307.9 %	+158.3 %
------	------	------	------	----------	----------

To provide a global assessment of the model’s accuracy, three commonly used error metrics were computed. These metrics summarize the deviations between the predicted displacements and experimental measurements across all frequency points.

- Mean Absolute Error (MAE): the average absolute deviation between model predictions and experimental measurements.

$$MAE = \frac{1}{n} \sum_{i=1}^n |X_{\text{model},i} - X_{\text{exp},i}| \tag{2}$$

- Root Mean Square Error (RMSE): emphasizes large deviations by squaring errors.

$$RMSE = \sqrt{\frac{1}{n} \sum_{i=1}^n (X_{\text{model},i} - X_{\text{exp},i})^2} \tag{3}$$

- Mean Absolute Percentage Error (MAPE): evaluates the average relative error in percentage.

$$MAPE = \frac{100}{n} \sum_{i=1}^n \frac{|X_{\text{model},i} - X_{\text{exp},i}|}{X_{\text{exp},i}} \tag{4}$$

where n is the number of frequency points, $X_{\text{model},i}$ is the displacement predicted by the FEM model at the i -th frequency (either our model or Koike et al.’s), and $X_{\text{exp},i}$ is the corresponding experimental measurement.

Table 3. Global error metrics for umbo and stapes displacements relative to the experimental data of Gyo et al. [13].

Structure	Metric	Our model	Koike et al.
Umbo	MAE (nm)	3.83	5.23
	RMSE (nm)	4.35	5.63
	MAPE (%)	57.6	88.4
Stapes	MAE (nm)	1.88	2.39
	RMSE (nm)	2.03	2.60
	MAPE (%)	107.7	110.6

The pointwise deviations (Tables 1 and 2) indicate that our model generally follows Gyo et al.’s experimental measurements more closely, particularly within the critical frequency range of 700–2000 Hz, corresponding to the primary resonance of the tympano-ossicular chain.

The global error metrics (Table 3) confirm this trend: for the umbo, our model exhibits a lower MAE (3.83 nm vs. 5.23 nm for Koike et al.) and a reduced RMSE (4.35 nm vs. 5.63 nm). A similar trend is observed for the stapes footplate (MAE = 1.88 nm vs. 2.39 nm; RMSE = 2.03 nm vs. 2.60 nm). In terms of frequency, our model is closer to the experimental data at 8 out of 10 points for the umbo and 7 out of 10 points for the stapes.

The larger deviations observed above $\sim 1600\text{--}2000$ Hz, particularly for the stapes footplate, are mainly due to the absence of a detailed inertial loading of the cochlear fluid (intracochlear mass) and the simplification of damping. At high frequencies, the system's behavior is dominated by mass effects and higher-order structural modes that are highly sensitive to fine anatomical details.

The MAPE becomes very high for the stapes at high frequencies due to extremely small experimental displacements (<1 nm), which artificially inflate the percentage error. Therefore, assessing model accuracy at these frequencies should rely on MAE and RMSE rather than MAPE alone.

These results confirm that the CT-based FEM model reproduces experimental data more accurately than Koike et al.'s model across the studied frequency range. It is particularly reliable within the clinically critical range of $700\text{--}2000$ Hz and provides a robust tool for applications in auditory mechanics, diagnostics, pre-operative simulation, and prosthesis design. Future improvements should focus on fluid–structure coupling with the cochlea, frequency-dependent damping, and non-uniform tympanic membrane modeling.

4 CONCLUSION

In this study, a detailed three-dimensional finite element model of the human middle ear was developed based on high-resolution CT imaging. The model accurately represents the key structures, including the external auditory canal, tympanic membrane, ossicular chain, and associated ligaments and tendons. Validation against experimental data from Gyo et al. [13] and numerical results from Koike et al. [4] demonstrated that the CT-based FEM model reliably reproduces the vibratory behavior of the umbo and stapes footplate, particularly within the clinically critical frequency range of $700\text{--}2000$ Hz.

Quantitative comparisons show that the model achieves lower mean absolute errors (MAE) and root mean square errors (RMSE) than Koike et al.'s model, indicating closer alignment with experimental measurements. Discrepancies at higher frequencies ($>1600\text{--}2000$ Hz) are primarily due to the absence of detailed cochlear fluid inertial loading and the simplification of damping in the current model.

Overall, the model provides a robust and anatomically coherent tool for studying middle ear mechanics. It is suitable for applications in auditory diagnostics, pre-operative surgical planning, prosthesis design, and further biomechanical investigations. Future work should focus on integrating fluid–structure interactions of the cochlea, frequency-dependent damping, and non-uniform tympanic membrane modeling to further improve high-frequency accuracy and physiological realism.

References

- [1] M. K. Brummund, F. Sgard, Y. Petit, F. Laville, and H. Nélisse, “An Axisymmetric Finite Element Model to Study the Earplug Contribution to the Bone Conduction

- Occlusion Effect,” *Acta Acustica united with Acustica*, vol. 101, no. 4, pp. 775–788, Jul. 2015, doi: 10.3813/AAA.918872.
- [2] F. Sgard, “A 2D axisymmetric finite element model to assess the contribution of in-ear hearing protection devices to the objective occlusion effect”.
- [3] G. Viallet, F. Sgard, F. Laville, and J. Boutin, “Axisymmetric versus three-dimensional finite element models for predicting the attenuation of earplugs in rigid walled ear canals,” *J. Acoust. Soc. Am.*, vol. 134, no. 6, pp. 4470–4480, Dec. 2013, doi: 10.1121/1.4826182.
- [4] T. Koike, H. Wada, and T. Kobayashi, “Modeling of the human middle ear using the finite-element method,” *J. Acoust. Soc. Am.*, vol. 111, no. 3, pp. 1306–1317, Mar. 2002, doi: 10.1121/1.1451073.
- [5] Q. Sun, K.-H. Chang, K. J. Dormer, R. K. Dyer, and R. Z. Gan, “An advanced computer-aided geometric modeling and fabrication method for human middle ear,” *Medical Engineering & Physics*, vol. 24, no. 9, pp. 595–606, Nov. 2002, doi: 10.1016/S1350-4533(02)00045-0.
- [6] R. Z. Gan, B. Feng, and Q. Sun, “Three-Dimensional Finite Element Modeling of Human Ear for Sound Transmission,” *Ann. Biomed. Eng.*, vol. 32, no. 6, pp. 847–859, Jun. 2004, doi: 10.1023/B:ABME.0000030260.22737.53.
- [7] S. Elghanaoui, S. Assif, A. Faiz, and A. Hajjaji, “Numerical Modeling of Sound Transmission in the Human Ear Using Finite Element Analysis: Integration of Lumped-Parametric Model,” in *Proceedings of the 6th International Conference on Advanced Materials for Photonics, Sensing, and Energy Applications*, Y. Boughaleb, A. Hajjaji, E.-K. Hlil, and S. Laasri, Eds., Singapore: Springer Nature, 2025, pp. 549–562. doi: 10.1007/978-981-96-6378-1_34.
- [8] J. Zhang, J. Tian, N. Ta, and Z. Rao, “Transient response of the human ear to impulsive stimuli: A finite element analysis,” *J. Acoust. Soc. Am.*, vol. 143, no. 5, pp. 2768–2779, May 2018, doi: 10.1121/1.5026240.
- [9] C. Lee, P. Chen, W. Lee, J. Chen, and T. Liu, “Three-Dimensional Reconstruction and Modeling of Middle Ear Biomechanics by High-Resolution Computed Tomography and Finite Element Analysis,” *The Laryngoscope*, vol. 116, no. 5, pp. 711–716, May 2006, doi: 10.1097/01.mlg.0000204758.15877.34.
- [10] R. Z. Gan, F. Yang, X. Zhang, and D. Nakmali, “Mechanical Properties of Stapedial Annular Ligament,” *Med. Eng. Phys.*, vol. 33, no. 3, pp. 330–339, Apr. 2011, doi: 10.1016/j.medengphy.2010.10.022.
- [11] N. Elkhouri, H. Liu, and W. R. J. Funnell, “Low-Frequency Finite-Element Modeling of the Gerbil Middle Ear,” *JARO*, vol. 7, no. 4, pp. 399–411, Nov. 2006, doi: 10.1007/s10162-006-0055-6.
- [12] S. Assif, A. Faiz, C. Aziz, P. Komgue L.B, and A. Hajjaji, “Validation using the in vivo experiment of the 3D model of the human ear using the equivalent mechanical impedance of the Mass-Spring-Damper System,” *Eur. Phys. J. Appl. Phys.*, vol. 97, p. 74, 2022, doi: 10.1051/epjap/2022220170.
- [13] K. Gyo, H. Aritomo, and R. L. Goode, “Measurement of the Ossicular Vibration Ratio in Human Temporal Bones by Use of a Video Measuring System,” *Acta Oto-Laryngologica*, vol. 103, no. 1–2, pp. 87–95, Jan. 1987, doi: 10.3109/00016488709134702.

- [14] J. P. Wilson, “Mechanics of middle and inner ear,” *British Medical Bulletin*, vol. 43, no. 4, pp. 821–837, 1987, doi: 10.1093/oxfordjournals.bmb.a072220.